IL17A CRITICALLY SHAPES THE TRANSCRIPTIONAL PROGRAM OF FIBROBLASTS IN PANCREATIC CANCER AND SWITCHES ON THEIR PRO-TUMORIGENIC FUNCTIONS

UNIVERSITÀ DEGLI STUDI DI TORINO

IL17A critically shapes the transcriptional program of fibroblasts in pancreatic cancer and switches on their pro-tumorigenic functions.

Gianluca Mucciolo[a,b], Claudia Curcio[a,b], Cecilia Roux[a,b], Wanda Y. Li[c], Michela Capello[d], Roberta Curto[a,b], Roberto Chiarle[a,b,e], Daniele Giordano[a], Maria Antonietta Satolli[f], Rita Lawlor[g,h], Aldo Scarpa[g,h], Pavol Lukac[i], Dmitry Stakheev[i,j] Paolo Provero[b], Luca Vannucci[i], Tak W. Mak[c,k,l,m,1], Francesco Novelli[a,b,n,1] and Paola Cappello[a,b,n,1]

[a]Laboratory of Tumor Immunology, Center for Experimental Research and Medical Studies (CERMS), Città della Salute e della Scienza di Torino, and [b]Department of Molecular Biotechnology and Health Sciences, University of Torino, Torino, 10126, Italy; [c]Campbell Family Institute for Breast Cancer Research, Princess Margaret Cancer Centre, Toronto, ON M5G2M9, Canada; [d]Department of Clinical Cancer Prevention, The University of Texas MD Anderson Cancer Center, Houston, TX 77030, USA; [e]Department of Pathology, Boston Children's Hospital, Harvard Medical School, Boston, MA 02115, USA; [f]Medical Oncology Division, Centro Oncologico Ematologico Subalpino (COES), Città della Salute e della Scienza di Torino, Department of Oncology, University of Turin, Torino 10126, Italy; [g]ARC-NET Research Center, University of Verona, Verona 37134, Italy; [h]Department of Diagnostics and Public Health, University of Verona, Verona 37134, Italy; [i]Laboratory of Immunotherapy, Institute of Microbiology v.v.i., Czech Academy of Sciences, Prague 4-14220, Czech Republic; [j]Faculty of Medicine of the Charles University, Prague 2- 121 08, Czech Republic; [k]Department of Medical Biophysics, University of Toronto, Toronto, ON M5G 1L7, Canada; [l]Department of Immunology, University of Toronto, Toronto, ON M5S 1A8, Canada; [m]Department of Medicine, University of Hong Kong, 120 Pok Fu Lam Road, Hong Kong; [n]Molecular Biotechnology Center, University of Torino, Turin 10126, Italy.

[1]Corresponding e-mail addresses: tak.mak@uhnresearch.ca, or franco.novelli@unito.it, or paola.cappello@unito.it

Classification: Contributed Research article

Word count:

Key words: IL17A; pancreatic cancer; cancer-associated fibroblast; extracellular matrix; fibrosis

Abstract

A hallmark of cancer, including pancreatic ductal adenocarcinoma (PDA), is a massive stromal and inflammatory reaction. Many efforts have, therefore, been made to identify the anti- or pro-tumoral role of cytokines and immune subpopulations dispersed within the stroma. In this study, we have investigated the role of IL17A and its effect on tumor fibroblasts and, consequently, on the tumor microenvironment.

KPC mice that spontaneously developed PDA, due to the pancreas specific expression of *Trp53*^{R172H} and *Kras*^{G12D}, were crossed with IL17A knockout mice. KPC/IL17A$^{-/-}$ mice showed an extensive desmoplastic reaction, which did not impair a great immune infiltrate. Both macrophages, especially CD80^{+} and T cells, were more abundant at the earlier time point. Regarding T cells, a decrease in FoxP3^{+} cells and an increase in CD8^{+} T cells were observed in KPC/IL17A$^{-/-}$ mice compared to KPC/IL17A$^{+/+}$ mice. Fibroblasts isolated from IL17A$^{+/+}$ and IL17A$^{-/-}$ KPC mice revealed very different mRNA and protein profiles. IL17A$^{-/-}$ fibroblasts displayed the ability to restrain tumor cell invasion by producing factors involved in extracellular matrix remodeling and by increasing T cell recruitment. In particular, IL17A$^{-/-}$ fibroblasts produced higher levels of cytokines and chemokines favoring T helper 1 cell recruitment and activation, and lower levels of those recruiting myeloid/granulocytic immune cells. Single-cell quantitative PCR was performed with isolated fibroblasts and confirmed a very divergent profile of IL17A proficient and deficient cells. All these features can be ascribable to increased levels of IL17F observed in the sera of mice lacking IL17A, and to the higher expression of its cognate receptor (IL17RC) specifically in CAF IL17A$^{-/-}$. In addition to the known effects on neoplastic cell transformation, the IL17 cytokine family uniquely affects fibroblasts, and represents a suitable candidate target for combinatorial immune-based therapies in PDA.

Significance of this study

There is controversial data about the pro-tumoral role of pancreatic cancer stroma, and dissecting multiple aspects will help to develop effective tailored therapies. IL17A has been reported to accelerate the pancreatic acinar-ductal metaplasia, be important for maintaining stem-like cancer cells and recruit immunosuppressive granulocytes into the tumor.

Here we unveil a novel relationship between IL17A and pancreatic stromal cells, which strongly modifies their gene and protein expression profiles. Ablation of IL17A, in fact, modifies the cytokines/factors released by tumor fibroblasts by limiting T cell immunosuppression.

IL17A inhibition may represent an important tool for designing novel combined therapeutic approaches.

Introduction

A histological hallmark of pancreatic ductal adenocarcinoma (PDA) is pronounced desmoplasia. This derives from pancreatic stellate cells (PSC) activated to proliferate and produce collagens, laminin, and fibronectin, which differentially shape the stroma(1). The stroma also harbors infiltrative macrophages and inflammatory cells with the potential to suppress anti-tumoral immune mechanisms(2).

Although PDA is considered a "cold tumor" or "immune privileged site", it engages the immune system from its inception. Initially, cells of the innate system, such as macrophages and mast cells, are mainly involved(3). However, even early on, cells of adaptive immunity, particularly T cells are also engaged(4). Higher levels of tumor-infiltrating CD4 and CD8 lymphocytes and dendritic cells positively correlate with longer survival after surgical resection(5). We have recently reported that PDA-infiltrating lymphocytes specifically recognize PDA-associated antigens, but are often impaired in their effector functions due to the presence of regulatory T (Treg) cells(6) and macrophages(7). Levels of T helper 17 (Th17) cells and IL17 were also found to be elevated in pancreatic immune-infiltrates from humans as well as from mice (8), and their increase is Kras-dependent.

Until recently, treatment was designed to either limit the inflammatory response or deplete the stroma to enhance drug delivery to the cancer cells, while disrupting deleterious stroma-cancer cell interactions. A lot of data seems to support this hypothesis, but further investigations are needed, as tumor-restraining and -promoting functions of stroma have been described(9). In pancreatic cancer, IL17, produced by classical αβ but also γδ T cells, neutrophils and myeloid cells, has been described involved in the acinar-ductal metaplasia and metastasis(10, 11), in the re-differentiation of pancreatic cancer cells in stem-like cells(12), and more recently in modulating neutrophil recruitment into pancreatic cancer with the consequence cytotoxic CD8 T cell exclusion(8). In addition, a Th2- and Th17-skewed response was associated with a paucity of dendritic cells (DC) that infiltrate PDA at an early stage of disease, and faster tumor progression(13). In this study, we investigated the role of IL17A in modulating PDA-associated stromal cells in a spontaneous mouse model that faithfully

recapitulates human PDA progression (KPC mice) crossed with IL17A knock-out mice. We observed a strong fibrotic reaction and matrix deposition in PDA from KPC/IL17A$^{-/-}$ mice, which paralleled higher infiltration of CD3^{+} T cells and, in particular, CD8^{+} T cells. The transcriptomic and secretome analysis of fibroblasts isolated from PDA arose in KPC/IL17A proficient or deficient mice revealed a different pattern of cytokine/chemokine production in the absence of IL17A, which suggests a shift from an immunosuppressive to an anti-tumoral microenvironment. Our results provide new insights into dissecting the role of IL17 family in PDA progression, which open the possibilities of designing combinatorial therapies for this deadly disease.

Results

The absence of IL17A increases the desmoplastic reaction at the tumor site.

PDA patients and mice spontaneously developing PDA, namely KC and KPC mice(14), displayed a trend of increase of IL17A-secreting CD4 T cells, and significantly higher IL17A in the sera, compared to healthy non-tumor counterparts (*SI Appendix, Table S1 and Fig. S1*). In addition, in mice, the frequency of Th17 was higher in the first weeks of age (*SI Appendix, Fig. S1B*). The increase of IL17A is Kras-dependent, as was observed only in presence of mutated Kras and/or TP53 but not in age-matched mice carrying the Pdx-1-Cre recombinase alone (*SI Appendix, Fig. S1C*). The high levels of IL17A in mouse sera at the late stage of disease, despite the decrease in IL17A-producing cells in the blood, may reflect the high secretion of this cytokine by other cells, such as γδ T cells (mainly producers), NKT cells, neutrophils and myeloid cells, which are dispersed into the tumor or lymphoid organs. These results prompted us to evaluate the progression of PDA in the absence of IL17A.

KPC mice were bred with IL17A$^{-/-}$ mice(15) to create a spontaneous autochthonous mouse model of PDA developing in the genetic absence of IL17A. KPC/IL17A$^{-/-}$ mice showed a significantly prolonged survival compared to the proficient KPC mice (*SI Appendix, Fig. S2A*). However, when pancreatic tissues were histologically analyzed, no differences were observed in terms of percentage of tumors (*SI Appendix, Fig. S2B and C*). Analyzing the expression of the different receptors for the IL17 family members, PDA cells from KPC/IL17A$^{-/-}$ mice expressed more IL17RA, the common chain, but less IL17RC, which dimerizes with the IL17RA to bind homo- and hetero-dimers of IL17A and IL17F (*SI Appendix, Fig. S2D*). Notably, we observed higher levels of IL17F in the sera of KPC/IL17A$^{-/-}$ mice compared to the proficient KPC, but no differences were observed in the single mutated model KC (*SI Appendix, Fig. S1E and F*). Tumor cells from KPC/IL17A$^{-/-}$ mice also expressed less IL17RE, the ligand of which is IL17E or IL25 that shares less homology with the other members of the family, and more IL17RD the ligand of which is unknown, and has been suggested to bind IL17A but not IL17F (*SI Appendix, Fig. S2D*). Both IL17A-proficient and IL17A-deficient

PDA cells produce very little IL17F, if any (*SI Appendix, Fig. S2E*). These data suggest that tumor cells in the absence of IL17A have a decrease in the receptor chains binding IL17F, and may be less responsive to this cytokine, which concomitantly increases. When we histologically analyzed the tumors that arose in KPC IL17A-proficient and -deficient mice, KPC/IL17A$^{-/-}$ mice displayed a significantly higher percentage of fibrosis compared to IL17A-proficient mice at every time point (Fig 1*A and B*). Multiphoton confocal microscopy imaging by second harmonic generation (SHG) revealed a structurally different collagen texture in KPC/IL17A$^{-/-}$ mice compared to IL17A-proficient controls (Fig 1*B* lower panels). In particular, the absence of IL17A led to the formation of less compact, more fibrillar net-like structures around the tumor and in the peri-tumoral area, with a tendency of greater involvement of the tissue (collagen in yellow). Notably, as shown in the lower right panels, KPC/IL17A$^{-/-}$ mice also displayed a normal acinar area surrounded by intense fibrosis (Fig. 1*B*). In addition, analysis of SHG imaging revealed that the integrated density (referred to as intensity of signal due to collagen fiber thickness and/or accumulation), was higher in the KPC/IL17A$^{+/+}$ tissues even in the presence of a similar total area of collagen occupation, which actually increased in KPC/IL17A$^{-/-}$ mice at 20 weeks of age (*SI Appendix Fig. S3A and B*). This was also supported by the average size of fibers, obtained by measuring the single dots in which the full collagen image, resulting from the detected SHG signal above the background threshold, being fragmented. This size was evidently higher in KPC/IL17A$^{+/+}$ pancreas at a later stage (at 20 weeks) (*SI Appendix Fig. S3C*). These data also suggest a progressive increase of stiffness in the presence of IL17A, because of the accumulation and increasing thickening of the collagen structure, which is opposite to the more diffuse and less dense accumulation in pancreas in the absence of IL17A.

Interestingly, PDA patients with high levels of IL17A in their sera (N = 10, *SI Appendix Table S1*) displayed wide and strengthened collagen fibers interspersed in the matrix and tumor cells similarly to KPC/IL17A$^{+/+}$ mice. By contrast, PDA patients with low levels of IL17A (N = 10) displayed softer collagen fibers, as observed in KPC/IL17A$^{-/-}$ mice (Fig. 1*C*). To classify patients with high or low levels of IL17A in their sera, we established a cut-off level that corresponded to the average amount

of IL17A plus twice the SD detected in the sera of healthy subjects (55 pg/ml). Therefore, the absence of IL17A led to more extensive desmoplasia, but much less compact and fibrillar-like collagen texture.

The absence of IL17A influences the anti-tumoral phenotype of fibroblasts.

To evaluate the role of IL17A in influencing tumor fibroblasts, we isolated cancer-associated fibroblasts (CAFs) from KPC/IL17A$^{+/+}$ and KPC/IL17A$^{-/-}$ mice, and analyzed for typical stromal cell markers and their responsiveness to recombinant IL17A (rIL17A) (*SI Appendix, Fig. S4A-C*). We also isolated normal fibroblasts (NF) from the pancreas of non-tumor-bearing IL17A-proficient and -deficient mice to compare as baseline, whilst remaining aware of the bias of stimulating all these cells toward a myofibroblastic phenotype(16) by culturing them on plastic supports. Due to the increased IL17F levels in the sera of tumor-bearing mice, we also evaluated the expression of all the members of the IL17R family and the production of IL17F from CAFs and NFs (*SI Appendix, Fig. S4D and E).* In the absence of the IL17A gene, the IL17R family was present at similar levels observed in IL17A-proficient CAFs and NFs, with the exception of IL17RB, which seemed absent or undetectable in all cells, and the IL17RC chain, which was significantly more expressed in CAFs/IL17A$^{-/-}$ compared to CAFs/IL17$^{+/+}$, and compared to both IL17A-proficient and -deficient NFs (*SI Appendix, Fig. S4D*). As expected, all CAFs and NFs produced little IL17F (*SI Appendix, Fig. S4E*). These data suggest that CAFs could be more responsive to IL17F in the absence of IL17A, due to the higher expression of its receptor.

mRNA was purified to evaluate gene expression by qPCR, with a customized plate having 87 unique genes related to fibrosis, and supernatants were collected to evaluate the secretion of more than 100 cytokines/chemokines and soluble factors. *SI Appendix Fig. S5A and B* shows two heat maps obtained from the unsupervised hierarchical analysis of RNA, and protein expressions of IL17A$^{+/+}$ CAFs, IL17A$^{-/-}$ CAFs and IL17A$^{-/-}$ CAFs stimulated with rIL17A. The absence of IL17A strongly modulated 65 transcripts (*SI Appendix Fig. S5A* and Fig. *1D*); in particular, 15 were down-regulated (<0.5) and

50 were up-regulated (>2) in IL17A$^{-/-}$ CAFs compared to IL17A$^{+/+}$ CAFs. Genes up-regulated by more than 50-fold included collagen type I (*Col1a1*), metalloproteases (*Mmp2, Mmp9*), fibroblast growth factor (*Fgf*)-*2*, hepatocyte growth factor (*Hgf*), insulin growth factor (*Igf*)-1, chemokine *Cxcl10, Cxcl12* and *Ccl5*, and interferon (*Ifn*)-*γ*. The propensity of IL17A$^{-/-}$ CAFs to reshape the matrix was also suggested by the up-regulation of transcripts of tissue inhibitor metalloproteases (*Timp*)-*3* (25-fold), *Serpin1* (13.4-fold) and plasminogen activators, namely *Plau* and *Plat* (6.3- and 6.7–fold, respectively). Activation of the Tgfβ pathway was confirmed by the up-regulation of its receptor (*Tgfβr2*) and *Smad2, 3* and *4* transcripts (from 2- to 10-fold), as well as TGFβ-induced genes (e.g. *Ctgf, Col1A1, Cxcl12*), although the *Tgfb* transcript itself was down-regulated (0.5-fold). Noteworthy, many cytokine transcripts were also upregulated: *Il12a* and *Il12b, Il1b, Il6*, *Ifn-γ*, interferon regulatory factor (*Irf*)-*1*, and tumor necrosis factor (*Tnf*)-*α* (Fig. *1D*). Notably, *Ifn-γ*, *Il12* and *Il1b*, were not amplified at all in any IL17A$^{+/+}$ CAFs. Ingenuity Pathway Analysis (IPA) by using genes significantly up- and down-modulated suggested that one of the top upstream regulators of genes modulated in the absence of IL17A (besides TGFβ) was indeed IFN-γ (p-value = 1.22 x 10^{-34}) (Fig. *1E*). IPA also confirmed activation of the Th1 pathway (*Z* score = 1.67, p-value = 4.8x10^{-6}), NFkB (*Z* score = 1.63, p-value = 2.7x10^{-5}), DC maturation (*Z* score = 1.41, p-value = 0.3x10^{-8}) and the inhibition of the Th2 pathway (Z score = -2, p-value = 1.9x10^{-4}) in the absence of IL17A. Interestingly, although clustered together by the unsupervised hierarchical analysis, NFs from IL17A$^{-/-}$ mice displayed 23 up-regulated transcripts and 13 down-regulated transcripts compared to IL17A-proficient NFs (*SI Appendix, Fig. S5C*). In addition, fold-change of transcripts related to Th1 recruitment and activation, matrix remodeling and cell growth, which was increased in IL17A$^{-/-}$ CAFs compared to IL17A$^{+/+}$ CAFs, was also higher in IL17A$^{-/-}$ CAFs compared to IL17A$^{-/-}$ NFs. In parallel, fold-change of transcripts related to myeloid/granulocyte recruitment and activation, which was lower in IL17A$^{-/-}$ CAFs compared to IL17A$^{+/+}$ CAFs, was also reduced in IL17A$^{-/-}$ CAFs versus IL17A$^{-/-}$

NFs (*SI Appendix, Fig. S5E*). These data suggest that the absence of IL17A does not substantially influence normal fibroblasts, whereas it critically affects CAF functions.

Adding rIL17A to IL17A$^{-/-}$ CAFs significantly modulated 45 transcripts, specifically, 29 were downregulated and 16 were upregulated (*SI Appendix Fig. S5A* and Fig. *1D*). Almost all the highly upregulated transcripts induced by the absence of IL17A were downregulated by adding rIL17A, with the exception of *FgfR2* and *Igf-2*, which were further increased. All genes related to matrix remodeling were down-modulated, along with transcripts for Th1 cytokines, namely *Il12a, Il12b, Ifn-γ* and *Tnf-α* (neither *Il12a* nor *b* was amplified, and *Ifn-γ* and *Tnf-α* were down-regulated by 0.31- and 0.23-fold, respectively). Conversely, transcripts for granulocyte and monocyte-colony stimulating factor (*Gm-csf*) and granulocyte-colony stimulating factor (*G-csf*), and for the chemokine *Cxcl1* recruiting myeloid and granulocyte cells, were restored (3.6-, 4- and 11-fold, respectively) (Fig. *1D*).

Cytokine arrays were performed with supernatants from three different CAF bulks of each genotype, and from three IL17A$^{-/-}$ CAF bulks stimulated with rIL17A. A total of 57 proteins among the 144 tested were affected by ±30% due to the absence of IL17A; 32 proteins were down-regulated and 25 were up-regulated (Fig. *1D* and *SI Appendix Fig. S5B*). Most of the upregulated proteins were chemokines attracting dendritic cells (e.g. CCL9; 2.35-fold) and T cells. Among them, CXCL9, CXCL12 and CCL5 were the most upregulated, increasing by about 1.9-, 1.4- and 4.5-fold, respectively. Notably, IL12 was upregulated by 70% in the supernatants of IL17A$^{-/-}$ CAFs, while Pentraxin3 and osteoprotegerin, which are usually regulated by TNF-α, were upregulated by about 30%. Interestingly, all factors mobilizing and differentiating granulocyte and myeloid precursors (GM-CSF, G-CSF, M-CSF and Flt3) were downregulated in the absence of IL17A, whereas the SCF (KITLG) protein, normally produced by fibroblasts and endothelial cells and very similar to Flt3, but with the specific ability to affect mast cells, was upregulated by 2-fold (Fig. *1D*). Insulin growth factor binding protein (IGFBP)-6 was the most upregulated protein (by 87-fold); IGFBP-6 binds IGFs with a higher affinity to IGF-2 than IGF-1, thus acting as a negative regulator(17) (Fig. *1D*). Cytokine

array analysis with supernatants from both IL17A-proficient and deficient NFs revealed fewer differences between the two normal fibroblasts compared to that highlighted by the transcriptome analysis (*SI Appendix Fig. S5D*). Again, however, fold-changes of proteins related to Th1 recruitment and activation, which were increased in IL17A$^{-/-}$ CAFs compared to IL17A$^{+/+}$ CAFs, were also higher in IL17A$^{-/-}$ CAFs compared to IL17A$^{-/-}$ NFs. In parallel, fold-changes of proteins related to the myeloid/granulocyte recruitment and activation, which were lower in IL17A$^{-/-}$ CAFs compared to IL17A$^{+/+}$ CAFs, were also decreased in IL17A$^{-/-}$ CAFs versus IL17A$^{-/-}$ NFs (*SI Appendix, Fig. S5E*). Adding rIL17A to IL17A$^{-/-}$ CAFs resulted in the modulation of 68 proteins; 40 proteins were downregulated and 28 were upregulated. Notably, most of the proteins were inversely regulated by the presence of rIL17A, as highlighted by the heat map (Fig. *1D* and *SI Appendix Fig. S5B*).

We then investigated a PDA cohort in *The Cancer Genome Atlas* for genes related to the Th1 response and myeloid and granulocyte cell recruitment based on those enhanced or down-regulated in the absence of IL17A, as reported in Fig. *1D*. The first group of genes, related to Th1 responses and T cell movement, were amplified or transcripts were enhanced in PDA patients with a better overall survival (Fig. *1F* left panel). Conversely, genes related to granulocyte/monocyte movement and cell-matrix interaction, which were significantly decreased in the absence of IL17A, were mutated, or transcripts were diminished in patients with a better overall survival (Fig. *1F*, right panel).

Overall, CAFs from IL17A$^{-/-}$ mice seemed more prone to matrix remodeling, favoring T cell recruitment, which, thanks to the cytokines released, namely CCL5, IL12 and IFN-γ, may be skewed to a Th1 phenotype and expand CD8 T cells.

IL17A affects fibroblast clustering based on transcriptional activity.

To further characterize CAF populations, we performed a single cell qPCR analysis with CAF bulks from KPC/IL17A$^{-/-}$ or KPC/IL17A$^{+/+}$ tumors. Despite the bias of performing a qPCR for 96 chosen genes, IL17A-proficient and -deficient CAFs clearly clustered into two different populations with 45 genes being differentially expressed between the two genotypes (Fig. 2*A* and *B* and *SI Appendix Table*

S5), mostly confirming previous results. Bioinformatics analysis also revealed that both CAF genotypes clustered into two different subpopulations (cluster 0 and 3 for IL17A$^{+/+}$ and 1 and 2 for IL17A$^{-/-}$; Fig. 2*A* and *B*). Of the 45 differentially expressed genes, five genes were only statistically different in cluster 0 vs 3 but not in cluster 1 vs 2; ten genes were statistically different in cluster 1 vs 2 but not 0 vs 3, and four genes were differentially expressed in both IL17A$^{+/+}$ and IL17A$^{-/-}$ clusters (Fig. 2*C*). A total of 37 genes were not significantly different in IL17A$^{-/-}$ vs IL17A$^{+/+}$ CAFs, but nine of them were differently expressed in clusters regardless of the presence of IL17A; nine were differentially clustering IL17A$^{-/-}$ CAFs, while only two were differentially clustering IL17A-proficient CAFs (Fig. 2*C*). Notably, we observed that only IL17A$^{-/-}$ CAFs strongly expressed *Cd34* gene suggesting a hematopoietic origin, but they also expressed high levels of *Acta2*, *Postn* and *Pdgfrb* along with *Col1a1* and *Col5a2,* usually expressed by fibroblasts (*SI Appendix Table S5*).

The absence of IL17A affects PDA cellular infiltrate.

To evaluate the presence of activated fibroblasts, macrophages and T cells, pancreatic tissues were analyzed by immunohistochemistry (IHC). In KPC mice, the absence of IL17A led to a huge increase in inter-dispersed αSMA^{+} cells and all around the tumor area, especially when invasive PDA was well established (Fig. *2D*). There were more macrophages, evaluated as F4/80^{+} cells, in KPC/IL17A$^{-/-}$ mice at 12 weeks of age (first time point analyzed), but they reached a similar score at later time points compared to the proficient counterparts (Fig. *2E*). Interestingly, among macrophages, CD80^{+} cells were significantly more abundant in KPC/IL17A$^{-/-}$ than in KPC/IL17A$^{+/+}$ tumors, while no significant changes were observed for the presence of CD163^{+} cells (*SI Appendix, Fig. S6*). Notably, we observed many more T cells (CD3^{+}) in KPC/IL17A$^{-/-}$ mice at earlier time points, but not at 20 weeks of age, because CD3^{+} levels in KPC/IL17A$^{+/+}$ mice increased to similar levels (Fig. *2F*). However, among these, FoxP3^{+} T cells significantly decreased in KPC/IL17A$^{-/-}$ mice when tumors were well-established compared to the proficient mice, despite being more abundant at early stages

(Fig. *2G*), and $CD8^+$ T cells were more numerous in KPC/$IL17A^{-/-}$ than in KPC/$IL17A^{+/+}$ mice at all time points (Fig. *2H*).

Overall, even in the presence of greater fibrosis, the absence of IL17A increased PDA immune cell infiltration by inflammatory-activated macrophages and effector CD4 and CD8 T cells.

The IL17A-dependent fibroblast phenotype shapes the anti-tumor T cell response and PDA cell invasion.

To assess if treatment with an anti-IL17A antibody (Ab) recapitulated features, in terms of gene expression and immune cell recruitment, observed in CAFs and tumors from KPC/$IL17A^{-/-}$ mice, C57/Bl6 mice were orthotopically injected with syngeneic PDA cells, and left untreated or treated with an anti-IL17A Ab biweekly. Treatment only slightly decreased the weight of tumors evaluated at 28 days after cell challenge (*SI Appendix, Fig. S7A*), probably due to the high rate of tumor growth and aggressiveness. No differences were observed in fibrosis or $aSMA^+$ cells for the surgical approach in the orthotopic injection (*SI Appendix Fig. S7B*). However, analyses by IHC of the immune infiltrate revealed a trend of increase in $CD3^+$ cells, and a parallel decrease in $FoxP3^+$ cells in mice treated with the anti-IL17A Ab, compared to control mice (*SI Appendix Fig. S7C and D*). mRNA extracted from paraffin-embedded pancreatic sections from KPC/$IL17A^{+/+}$, KPC/$IL17A^{-/-}$ and from mice injected orthotopically and left untreated or treated with the anti-IL17A Ab, were analyzed by qPCR (Fig. 3*A and B*). The absence of IL17A in KPC mice strongly upregulated transcripts associated with T cell activation after antigen recognition, namely *B2m, Nfatc* and *Calm3*, and with the effector T cell phenotype, such as *Gzmb, Il18, Fasl, Cd8, Jak1* and *Ccr5*. Notably, genes antagonizing the Th1 response such as *Rorc, Tgfb1, Tlsp* and *Il4* were downregulated by more than 100-fold (Fig. 3*A*). The increased transcripts of *Gzmb*, *Stat1*, *Fasl* and *B2m* also confirmed the "interferon signature" observed by analyzing the CAF transcriptome and secretome.

Notably, the anti-IL17A Ab treatment of mice orthotopically injected with syngeneic PDA cells demonstrated a transcript regulation pattern that suggested a microenvironment similar to that

observed in KPC/IL17A$^{-/-}$ mice (Fig. 3*B*). Indeed, the analysis of mRNA extracted from paraffin-embedded pancreatic sections revealed that stromal (*Cd36, Postn, Col1a1, aSma*), T cell chemoattracting (*Cxcl10, Cxcl11, Ccl5 and Ccr5*) and T cell activation (*Cd8, Nfkb, Nfatc, Gzmb*) related genes were significantly upregulated compared to those evaluated in untreated mice (Fig. 3*B*). To assess the role of IL17A-stimulated CAFs in modulating tumor cell behavior we cultured PDA cells with rIL17A or supernatants from IL17A$^{-/-}$ CAFs. Cell viability was not affected at all by the addition of rIL17A (*SI Appendix Fig. S8A*), while it only directly affected cell invasion after 24 h (*SI Appendix Fig. S8B*). Supernatants collected from all CAFs induced a similar rate of invasion after 24 h of culture, while IL17A$^{+/+}$ CAFs significantly increased the invasion by PDA compared to that from IL17A$^{-/-}$ CAFs and from IL17A$^{-/-}$ CAFs stimulated with rIL17A after 48 h, which, however, only induced a slight increase in the PDA invasion ability (*SI Appendix, Fig. S8C*). Evaluating some epithelial-to-mesenchymal transition (EMT) genes revealed the up-regulation of *Zeb* and *Snail* by rIL17A alone (1 ng and 10 ng/ml, respectively) and of *Zeb1*, *Slug* and *vimentin* by the addition of supernatants from IL17A$^{-/-}$ CAFs. Of note, the stimulation of IL17A$^{-/-}$ CAFs with rIL17A made them release some factors, which stimulated upregulation of all the EMT transcripts evaluated (*SI Appendix, Fig. S8D*). These results may partially explain the lower number of metastasis that we observed in KPC/IL17A-deficient mice, at later time points, and especially in the lungs (*SI Appendix Fig. S8E*).

Overall, these results supported the hypothesis that the absence of IL17A increases both fibrosis-associated genes, but also inflammatory-activated T cells. In addition, the absence of IL17A modifies CAFs for restraining tumor cell invasion.

Discussion

The present study was aimed at characterizing the role of IL17A in modulating fibroblasts associated with PDA, and consequently their role in supporting or suppressing the anti-tumor response. The most remarkable histological feature in our spontaneous mouse model of PDA lacking the IL17A gene was enhanced fibrotic reaction. This first observation is divergent from that observed after treatment with the combination of anti-IL17A, anti-IL17F and IL17RA antibodies(10). Of interest, IL17F increased in the absence of IL17A, and IL17RC was upregulated specifically on CAFs, but not PDA cells. This suggests that in the absence of IL17A, the interaction between IL17F and its receptor plays a role in differently modulating the tumor environment. Notably, this enhanced fibrosis seemed to have a "tumor-restrainer" function. Some stromal constituents, indeed, act to contain rather than promote tumor progression(18, 19), and recent studies have started to define the complex stromal population in greater depth(20, 21). Clinical studies employing patient biopsies also correlated the extent of desmoplasia, after stroma and collagen quantification, with a better prognosis(22–24). More recently, it has been observed that the lower density of tumor stroma corresponds to a higher cellularity in liver metastasis, which correlates with lower patient survival. In addition, the reduction of matrix in a PDA orthotopic mouse model through an anti-LOXL2 antibody decreased tissue stiffness, but increased tumor growth, and reduced gemcitabine responsiveness that negatively impacted on mouse survival(25). This highlights the need to systematically determine the effects of many soluble factors released by immune cells as well tumor cells on the activation of PDA stroma to improve the development of effective and "tailored" therapeutic strategies.

KPC/IL17A$^{-/-}$ mice displayed a less suppressive tumor microenvironment than that described for wild type mice(26); they were infiltrated to a much greater extent by CD3^{+}, CD8^{+} and F4/80^{+} cells, with a significant increase in CD80^{+} macrophages, despite the presence of abundant fibrosis and stroma, indicating an attempt by the immune system to mount an anti-tumor response. Acute and chronic pancreatitis in mice lacking NFkB essential modulator (NEMO) showed a similar pattern of inflammation and fibrosis observed in KPC/IL17A$^{-/-}$(27). It appears that the absence of certain

immune modulators, such as NEMO or IL17A, which also signal through NFkB, similarly increases the inflammatory response and exacerbates the fibrotic reaction in PDA.

Unsupervised hierarchical analysis of fibroblast transcript and secretome confirmed the similar origin of fibroblasts, clustering together CAFs and NFs. However, although many cytokines and chemokines have been described to be commonly secreted by normal activated fibroblasts and CAFs(28), the increase of T cell-recruiting chemokines and Th1-skewing cytokines in IL17A$^{-/-}$ CAFs suggests their role in promoting an effector inflammatory response, similar to that known to be induced after infection or cell injury. In tumors, this type of reaction may correspond to an anti-tumor immune response (Fig. 4). This hypothesis was confirmed by the Th1 and cytotoxic signature observed in tumors from KPC/IL17A$^{-/-}$ and anti-IL17A-treated mice compared to their proficient counterparts, as well as the activation of an "interferon signature", as revealed by *Gzmb, Fasl, Stat1* and *B2m* mRNA upregulation. The interferon signature and cytotoxic lymphocytes, in fact, are usually associated with a good cancer prognosis and can predict the response to immune check-point inhibitory therapies(29).

Single cell analysis of IL17A$^{+/+}$ and IL17A$^{-/-}$ CAFs confirmed the presence of two main subpopulations regardless of the presence or absence of IL17A, but more than half of the amplified genes were significantly different in IL17A$^{-/-}$ compared to proficient CAFs. Notably, the expression of *Cd34* by IL17A$^{-/-}$ cells only suggested the hematopoietic origin of these fibroblasts, which, however, also expressed higher or similar levels of genes usually associated with a fibroblast phenotype *(Acta2, Postn, Pdgfrb, Col1a1, Col5*, *Col4a1* and *Col4a2*). Of note, the loss of CD34 on stromal cells has been associated with the increased ability of breast cancer cells to invade surrounding tissues and metastasize(30), and has been defined as an independent prognostic factor in non-small cell lung cancer stage I-III(31). Interestingly, IL17A$^{+/+}$ CAFs also highly expressed *Anxa6* and *Areg*, which were almost absent in IL17A$^{-/-}$ CAFs. The former was demonstrated to be typical of stromal cells promoting tumors and metastasis(20), and the latter is an important factor supporting

tumor cells by increasing their survival, neoangiogenesis and recruitment of protumoral macrophages(32, 33).

Another set of genes, significantly modulated by the absence of IL17A, are those involved in extracellular matrix remodeling, and indirectly related to cellular invasion, which have been implicated in PDA progression and resistance to treatment. In line with this data, we observed a different structure and size of collagen fibers in PDA from IL17A$^{-/-}$ mice compared to those in proficient mice. In the absence of IL17A, collagen deposition is more orientated to form soft nests rather than compact capsules around tumor cells, as demonstrated by SHG microscopy and quantitative analysis of the integrated density. Collagen fiber organization correlates with the ability of tumor cells to invade, as straight aligned fibers represent paths on which cancer cells can move, and also influences the epithelial-to-mesenchymal transition (EMT)(34, 35). Therefore, our results highlight the formation of two functionally different scaffolds; the first, softer matrix allows immune cell accumulation and lowers the induction of tumor cell motility and, possibly, maintains better differentiation; the second, in IL17A-proficient mice, allows matrix stiffening with consequent hindrance of immune cell infiltration, but stimulates EMT, which promotes cell mobilization, infiltration and spreading(36).

Notably, some markers associated with PSC were more upregulated in IL17A$^{-/-}$ CAFs compared to IL17A$^{+/+}$ CAFs (*SI Appendix Fig. S4B*). This suggests a persistence or a tendency to renew these cells rather than their conversion into pro-tumoral myofibroblasts(16, 20). A link with the persistence of activated fibroblasts and PSC could be represented by the massive increase in IGFBP-6 secretion. IGFBP-6 overexpression is protective for fibroblasts as it markedly delays the onset of senescence(37). In addition, IGFBP-6 acts as a dominant negative regulator of the IGF pathway; therefore, in IL17A$^{-/-}$ mice, where IGFBP-6 is upregulated, it could prevent pro-tumorigenic effects of both IGF1 and IGF2(38), which are abundantly secreted by both stromal and tumor cells. By blocking this signaling, a fully human monoclonal antibody (IgG1) against IGF-1R, inhibits the

growth of pancreatic as well breast and renal tumors, and induces a marked increase in apoptotic tumor cells(39).

In conclusion, we demonstrate here that IL17A differently modulates stromal cells and creates a suppressive environment by recruiting granulocytes and myeloid suppressive cells, which - in turn - induces Treg cells and reduces the attempt of an efficient cellular anti-tumor response. The absence of IL17A, instead, did not limit stroma in PDA, but converted the immunosuppressive environment into an anti-tumoral one, as schematically represented in Fig. 4. Cytokines and chemokines produced by CAFs in the absence of IL17A favor the recruitment of Th1 and cytotoxic $CD8^+$ T cells, and limit the presence of suppressive myeloid cells and Treg. Our findings emphasize the importance of deep analyzing the tumor microenvironment to avoid the general elimination of stroma and fibroblasts, rather than modifying their function. Overall, identifying a novel relationship between IL17A and the stroma also provides a proof-of-concept for its inhibition in combined therapeutic strategies.

Materials and Methods

Human samples. Human PBMC and sera were isolated from PDA patients enrolled in the study known as PANIN (*SI Appendix Table S1*), previous informed consent was obtained, and the study was approved by the Ethical Committee (N. 2CEI/587) of the Città della Salute e della Scienza di Torino, Italy and of the Policlinico Hospital, Verona, Italy. Blood from healthy donors was obtained by the local Blood Bank.

ELISA. Human and mouse IL17A, and mouse IL17F were quantified in sera from healthy subjects, PDA patients and/ IL17A-proficient and -deficient or KC, KPC and Pdx-1-Cre mice (dilution 1:50 for IL17A or pure for mIL17F), by means of an ELISA assay, following the manufacturer's instructions (both from Biolegend by Prodotti Gianni).

Immunophenotyping. Detailed procedures of immunophenotyping can be found in the *SI Appendix*.

Mice. Generation and characterization of mice carrying double-mutated $Kras^{G12D}$ and $Trp53^{R172H}$ (KPC) under the endogenous promoter and flanked by Lox-STOP-Lox cassettes have been previously described(14). Mice were crossed with IL17A KO mice (kindly provided from Dr. Yoichiro Iwakura, University of Tokyo, Japan) to generate KPC/$IL17A^{-/-}$. Mice were screened by PCR using tail DNA amplified by specific primers to Lox-P cassette flanking Kras and WT Kras genes, Lox-P cassette flanking Trp53 mutated and WT Trp53 and Cre recombinase genes (14). For $IL17A^{-/-}$ mouse genotyping see *SI Appendix*.

Multiphoton Confocal Microscopy for Second Harmonic Generation (SHG) Imaging. All observations were performed at the 1- and 2-photon confocal microscopy at the facility of the Department of Biomathematics of the Institute of Physiology, Czech Academy of Sciences, using a

Leica TCSSP2 AOBS confocal laser scanning microscope (Leica, Wetzlar, GE) based on the Leica DM IRE2 inverted microscope, and equipped with an argon laser (40). For more details about the analysis and relative quantification see *SI Appendix*.

Cell lines and CAF isolation. Mouse PDA cell lines, derived from a KPC/IL17A$^{-/-}$ mouse at 20 weeks of age and a KPC/IL17A$^{+/+}$ mouse at 18 weeks of age, and fibroblasts - isolated as described below - were cultured in DMEM supplemented with 20 mM glutamine, 2% or 10% FBS, and gentamycin (40 μg/ml; Fisiopharma, Milan, Italy). All *in vitro* cultures were performed at 37°C in a humidified 5% CO_2 atmosphere.

Mouse CAFs were isolated from KPC/IL17A$^{+/+}$ and KPC/IL17A$^{-/-}$ mice with palpable PDA (28-20 weeks of age), and from non-tumor bearing IL17A$^{+/+}$ and IL17A$^{-/-}$ mice. Fibroblasts were isolated from tumoral and normal pancreas using a combination of outgrowth and clonal isolation after mechanical and enzymatic dissociation. See detailed procedures in *SI Appendix*. For some experiments, PDA cells and CAFs isolated from KPC/IL17A$^{-/-}$ mice were stimulated in the presence or absence of different concentrations of mouse rIL17A (1, 10 and 100 ng/ml; Abnova), and supernatants and cell pellets were collected and frozen until use.

Cytokine array and quantitative Real-Time PCR. Cytokines, chemokines, metalloproteases and growth factors were evaluated in the supernatants from CAFs obtained from KPC/IL17A$^{+/+}$ and KPC/IL17A$^{-/-}$ mice, and NFs from non-tumor bearing IL17A$^{+/+}$ and IL17A$^{-/-}$ mice with the mouse cytokine array C2000 (RayBiotech by Prodotti Gianni), which evaluates 144 factors, by following the manufacturer's instructions. For more details, see *SI Appendix*.

RNA from fibroblasts was obtained after lysis of frozen cell pellets using Nucleozol, or by processing paraffin-embedded tissues with the PureLink FFPE Total RNA isolation kit following the manufacturer's instructions (Invitrogen-ThermoFisher). iScript reverse transcription-kit (BioRad) was used to produce cDNA from 1μg of RNA, following the manufacturer's instructions. The qRT-

PCR reaction was performed using SYBR Green mix (Applied Biosystems by Thermo), and specific pairs of primers, or customized SYBR plates with unique 87 genes related to pancreatic fibrosis or T and B cell activation (*SI Appendix and Table S2 and S3*), and the SsoAdvance Universal SYBR green Supermix (both from BioRad) with the iQ96 machine or CFX1000 (BioRad). Gene expression was normalized to *Gapdh*.

Single-cell quantitative Real-Time PCR. Single-cell Real-Time qPCR was performed using the C1 Single-Cell Auto Prep System in tandem with the BioMark HD System (Fluidigm Corporation, Markham, ON, Canada), in the facility of the Campbell Family Institute for Breast Cancer Research (Toronto, Canada). Details and analyzed genes are listed in *SI Appendix and Table S4*.

Data and Single-cell qPCR analysis.

Genesis software (https://genome.tugraz.at/genesisclient/genesisclient_description.shtml; BG-IKD Software) was used to perform complete analysis of qPCR and cytokine array data; values were auto-scaled and the Pearson correlation was applied as the basis for distance measurement. Upstream regulator analysis was performed using the Ingenuity Pathway Analysis software (IPA; Ingenuity Systems, Redwood City, California). Genes and proteins to be differentially expressed in CAFs from KPC/IL17A$^{-/-}$, compared to both CAFs from KPC/IL17A$^{+/+}$ and KPC/IL17A$^{-/-}$ plus rIL17A, were imported for IPA analysis. Fold changes in KPC/IL17A$^{-/-}$ gene expression relative to KPC/IL17A$^{+/+}$ CAFs were measured. Significance was determined using the right-tailed Fisher exact test.

Seurat(41) was used to perform clustering and t-SNE dimensional reduction(42) of the single-cell expression data. The analysis was limited to genes expressed in at least three cells and cells expressing at least ten genes. This filter resulted in 358 cells and 82 genes being included in the analysis. Cluster markers and genes differentially expressed between the two genotypes were identified with a Mann-Whitney U test with Bonferroni correction for multiple testing.

Histology and Immunohistochemistry. Detailed methods of immunohistochemical analysis of CD3, CD8, CD80, CD163, F4/80, αSMA and FoxP3 can be found in the *SI Appendix*. The presence of positive cells was defined as absent (score 0.2), scarce (score 0.4), moderate (score 0.6), strong (score 0.8), and huge (score 1) on sections decorated with the different antibodies.

MTT and Matrigel-coated Transwell invasion assay. Cell survival was assessed by the MTT assay. PDA cells were seeded in a 96-well plate at $1.5x10^3$ cells/well, and 20 µl of 5 mg/ml MTT solution (Sigma-Aldrich) was added to each well, and incubated at 37°C for a further 4 h every 24 h. Plates were centrifuged for 10 min at room temperature and medium was removed. The insoluble formazan product was dissolved in 200 µl of dimethyl sulfoxide (Sigma-Aldrich) for 10 min at room temperature on a platform shaker. Optical density values were measured at 570 nm with a microplate reader (NIVO, PerkinElmer).

PDA cells seeded in triplicate on top of Matrigel-coated trans-wells were cultured with conditioned medium from unstimulated $IL17A^{+/+}$ or $IL17A^{-/-}$ CAFs or $IL17A^{-/-}$ CAFs stimulated with rIL17A (10ng/ml). After 48 h, cells were fixed with methanol, stained with methylene blue and dissolved in 5% acetic acid on a rotator for 15 min. A total of 100 µl of eluted cells were read at 570 nm wavelength with a microplate reader (NIVO, PerkinElmer).

Statistical analysis. The student's t-test, two-way ANOVA, Mann Whitney test and Chi-square test were used to evaluate the differences in all the experiments as indicated, with the exception of single-cell analysis, which is described separately above. All tests were performed with GraphPad Prism 8 Software, Inc. (San Diego, CA).

Author contributions

G.M., F.N., L.V., T.W.M. and P.C. designed the research; G.M., C.C., C.R., W.Y.Li, M.C., R.Cu., D.G., P.L., and P.C. performed the research; M.A.S., R.L., A.S., T.W.M., L.V. and F.N. provided reagents; G.M., C.C., M.C., R.Ch., L.V., P.P. and P.C. analyzed the data; T.W.M., L.V. and F.N. provided intellectual contributions and revised the data; G.M., L.V. and P.C. wrote the paper.

Acknowledgements

We thank Radhika Srinivasan and Thorsten Berger for carefully reading and editing our manuscript, and Prof. Yoichiro Iwakura, from the University of Tokyo, for kindly providing the IL17A$^{-/-}$ mice. We also thank Dr. O. Chernyavskiy, Institute of Physiology of the CAS, Prague, for technical support in confocal microscopy imaging procedures, and Federica Marchesi, Chiara Gorrini and Paola Nisticò for helpful discussion of results.

Funding

This work was supported by grants from the Associazione Italiana Ricerca sul Cancro (5 x mille no. 12182 and IG no. 15232, 19931) to AS and FN. Fondazione CRT (no. 2020.0719 to PC). University of Turin-Progetti Ricerca Locale (to FN and PC). Ricerca Finalizzata 2013 (no. 2013-02354892). Fondazione Onlus Ricerca Molinette (Fondo CD38 and Fondo Ursula e Giorgio Cytron). Associazione Nastro Viola. Fondazione Nadia Valsecchi. Institutional Grant (RVO 61388971) to LV. FP7 European Community Grant Cam-Pac (no: 602783) to AS and RTL.

Declarations of interest

The authors declare that there are no competing interests.

REFERENCES

1. M. V. Apte, J. S. Wilson, A. Lugea, S. J. Pandol, A starring role for stellate cells in the pancreatic cancer microenvironment. *Gastroenterology* **144**, 1210–9 (2013).
2. A. Neesse, H. Algul, D. A. Tuveson, T. M. Gress, Stromal biology and therapy in pancreatic cancer: a changing paradigm. *Gut* **64**, 1476–84 (2015).
3. G. L. Beatty, *et al.*, Exclusion of T Cells From Pancreatic Carcinomas in Mice Is Regulated by Ly6C(low) F4/80(+) Extratumoral Macrophages. *Gastroenterology* **149**, 201–10 (2015).
4. T. F. Gajewski, H. Schreiber, Y. X. Fu, Innate and adaptive immune cells in the tumor microenvironment. *Nat Immunol* **14**, 1014–22 (2013).
5. A. Fukunaga, *et al.*, CD8+ tumor-infiltrating lymphocytes together with CD4+ tumor-infiltrating lymphocytes and dendritic cells improve the prognosis of patients with pancreatic adenocarcinoma. *Pancreas* **28**, e26-31 (2004).
6. A. Amedei, *et al.*, Ex vivo analysis of pancreatic cancer-infiltrating T lymphocytes reveals that ENO-specific Tregs accumulate in tumor tissue and inhibit Th1/Th17 effector cell functions. *Cancer Immunol Immunother* **62**, 1249–60 (2013).
7. S. Borgoni, *et al.*, Depletion of tumor-associated macrophages switches the epigenetic profile of pancreatic cancer infiltrating T cells and restores their anti-tumor p... - PubMed - NCBI (May 24, 2018).
8. Y. Zhang, *et al.*, Interleukin-17–induced neutrophil extracellular traps mediate resistance to checkpoint blockade in pancreatic cancer. *J. Exp. Med.* **217** (2020).
9. C. Vennin, *et al.*, Reshaping the Tumor Stroma for Treatment of Pancreatic Cancer. *Gastroenterology* **154**, 820–838 (2018).
10. F. McAllister, *et al.*, Oncogenic Kras activates a hematopoietic-to-epithelial IL-17 signaling axis in preinvasive pancreatic neoplasia. *Cancer Cell* **25**, 621–37 (2014).
11. H. H. Wu, *et al.*, Targeting IL-17B-IL-17RB signaling with an anti-IL-17RB antibody blocks pancreatic cancer metastasis by silencing multiple chemokines. *J Exp Med* **212**, 333–49 (2015).
12. Y. Zhang, *et al.*, Immune Cell Production of Interleukin 17 Induces Stem Cell Features of Pancreatic Intraepithelial Neoplasia Cells. *Gastroenterology* (2018) https:/doi.org/10.1053/j.gastro.2018.03.041.
13. S. Hegde, *et al.*, Dendritic Cell Paucity Leads to Dysfunctional Immune Surveillance in Pancreatic Cancer. *Cancer Cell* **37**, 289-307.e9 (2020).
14. P. Cappello, *et al.*, Vaccination with ENO1 DNA prolongs survival of genetically engineered mice with pancreatic cancer. *Gastroenterology* **144**, 1098–106 (2013).
15. S. Nakae, *et al.*, Antigen-specific T cell sensitization is impaired in IL-17-deficient mice, causing suppression of allergic cellular and humoral responses. *Immunity* **17**, 375–87 (2002).
16. D. Ohlund, *et al.*, Distinct populations of inflammatory fibroblasts and myofibroblasts in pancreatic cancer. *J Exp Med* **214**, 579–596 (2017).
17. L. A. Bach, IGFBP-6 five years on; not so “forgotten”? *Growth Horm IGF Res* **15**, 185–92 (2005).
18. B. C. Ozdemir, *et al.*, Depletion of carcinoma-associated fibroblasts and fibrosis induces immunosuppression and accelerates pancreas cancer with reduced survival. *Cancer Cell* **25**, 719–34 (2014).
19. A. D. Rhim, *et al.*, Stromal elements act to restrain, rather than support, pancreatic ductal adenocarcinoma. *Cancer Cell* **25**, 735–47 (2014).
20. J. Leca, *et al.*, Cancer-associated fibroblast-derived annexin A6+ extracellular vesicles support pancreatic cancer aggressiveness. *J Clin Invest* **126**, 4140–4156 (2016).
21. E. Elyada, *et al.*, Cross-Species Single-Cell Analysis of Pancreatic Ductal Adenocarcinoma Reveals Antigen-Presenting Cancer-Associated Fibroblasts. *Cancer Discov.* **9**, 1102–1123 (2019).

22. K. M. Bever, *et al.*, The prognostic value of stroma in pancreatic cancer in patients receiving adjuvant therapy. *HPB* **17**, 292–8 (2015).
23. M. Sinn, *et al.*, alpha-Smooth muscle actin expression and desmoplastic stromal reaction in pancreatic cancer: results from the CONKO-001 study. *Br J Cancer* **111**, 1917–23 (2014).
24. M. Erkan, *et al.*, The activated stroma index is a novel and independent prognostic marker in pancreatic ductal adenocarcinoma. *Clin Gastroenterol Hepatol* **6**, 1155–61 (2008).
25. H. Jiang, *et al.*, Pancreatic ductal adenocarcinoma progression is restrained by stromal matrix. *J. Clin. Invest.* **130**, 4704–4709 (2020).
26. C. E. Clark, G. L. Beatty, R. H. Vonderheide, Immunosurveillance of pancreatic adenocarcinoma: insights from genetically engineered mouse models of cancer. *Cancer Lett* **279**, 1–7 (2009).
27. L. K. Chan, *et al.*, Epithelial NEMO/IKKgamma limits fibrosis and promotes regeneration during pancreatitis. *Gut* (2016) https:/doi.org/10.1136/gutjnl-2015-311028.
28. R. Kalluri, The biology and function of fibroblasts in cancer. *Nat Rev Cancer* **16**, 582–98 (2016).
29. F. Petitprez, *et al.*, Transcriptomic analysis of the tumor microenvironment to guide prognosis and immunotherapies. *Cancer Immunol Immunother* (2017) https:/doi.org/10.1007/s00262-017-2058-z.
30. X. Catteau, P. Simon, J.-C. Noël, Myofibroblastic stromal reaction and lymph node status in invasive breast carcinoma: possible role of the TGF-β1/TGF-βR1 pathway. *BMC Cancer* **14**, 499 (2014).
31. A. B. Schulze, *et al.*, Prognostic impact of CD34 and SMA in cancer-associated fibroblasts in stage I-III NSCLC. *Thorac. Cancer* **11**, 120–129 (2020).
32. S. Kubli, AhR controls redox homeostasis and shapes the tumor microenvironment in BRCA1-associated breast cancer.
33. C. Roux, *et al.*, Reactive oxygen species modulate macrophage immunosuppressive phenotype through the up-regulation of PD-L1. *Proc. Natl. Acad. Sci.*, 201819473 (2019).
34. C. R. Drifka, *et al.*, Highly aligned stromal collagen is a negative prognostic factor following pancreatic ductal adenocarcinoma resection. *Oncotarget*, 76197 (2016).
35. L. Vannucci, Stroma as an Active Player in the Development of the Tumor Microenvironment. *Cancer Microenviron.* **8**, 159–166 (2015).
36. T. J. Puls, X. Tan, C. F. Whittington, S. L. Voytik-Harbin, 3D collagen fibrillar microstructure guides pancreatic cancer cell phenotype and serves as a critical design parameter for phenotypic models of EMT. *PLOS ONE* **12**, e0188870 (2017).
37. L. Micutkova, *et al.*, Insulin-like growth factor binding protein-6 delays replicative senescence of human fibroblasts. *Mech Ageing Dev* **132**, 468–79 (2011).
38. E. K. Rowinsky, *et al.*, IMC-A12, a human IgG1 monoclonal antibody to the insulin-like growth factor I receptor. *Clin Cancer Res* **13**, 5549s–5555s.
39. D. Burtrum, *et al.*, A fully human monoclonal antibody to the insulin-like growth factor I receptor blocks ligand-dependent signaling and inhibits human tumor growth in vivo. *Cancer Res* **63**, 8912–21 (2003).
40. O. Chernyavskiy, *et al.*, Imaging of mouse experimental melanoma in vivo and ex vivo by combination of confocal and nonlinear microscopy. *Microsc. Res. Tech.* **72**, 411–423 (2009).
41. T. Stuart, *et al.*, Comprehensive Integration of Single-Cell Data. *Cell* **177**, 1888-1902.e21 (2019).
42. L. van der Maaten, G. Hinton, Visualizing Data using t-SNE. *J. Mach. Learn. Res.* **9**, 2579–2605 (2008).

Figure legends

Figure 1. IL17A affects fibrotic reactions in pancreatic cancer and differently shapes stroma. (*A*) Tumor pancreatic fibrosis quantification in KPC/IL17A$^{+/+}$ (white floating bars) and KPC/IL17A$^{-/-}$ (grey floating bars) mice. Each symbol corresponds to a single mouse analyzed with ImageJ (N = 5-8 mice/group), and min to max values are represented. *$P < 0.05$ and ***$P < 0.0001$ represent significant differences in the IL17A-deficient mice compared to the IL17A-proficient mice. (*B*) Representative pictures of PicroSirius Red staining (upper panels) and of SHG microscopy analysis (lower panels) of pancreatic tissues from KPC/IL17A$^{+/+}$ and KPC/IL17A$^{-/-}$ mice at the indicated age (N = 5-8 mice/group). The same areas were recorded in transmission light for PricoSirius Red staining and with the two-photon microscope for SHG, and collagen fibers are represented in yellow. Arrows indicate more dispersed and less compact collagen fibers, and arrowheads indicate straight and tight collagen fibers. Scale bar represents 75 μm. (*C*) Representative pictures of PicroSirius Red staining of pancreatic tissues from patients with high (left panels) and low (right panels) levels of serum IL17A. Magnification at 40X points out the differences in fibrillar structure. Scale bars represent 150 μm and 50 μm respectively at 10X and 40X magnification. (*D*) A close-up view of specific genes and proteins differentially expressed in the absence of IL17A. The most relevant factors related to myeloid/granulocyte recruitment and activation (upper left), Th1 recruitment and activation (lower left), matrix remodeling (upper right) and cell growth (lower right) are grouped into four blocks. The color code maps represent the fold-change in IL17A$^{-/-}$ CAFs versus IL17A$^{+/+}$ CAFs and in IL17A$^{-/-}$ CAFs stimulated with rIL17A (10 ng/ml) versus IL17A$^{-/-}$ CAFs, as indicated by each closed block (N=3 CAF bulk each). (*E*) Top upstream regulators predicted by IPA to be activated in the absence of IL17A. (*F*) Kaplan-Meier curves comparing survival of PDA patients from TCGA interrogation about genes found upregulated (Th1 response) or down-modulated (myeloid/granulocyte recruitment) in fibroblasts from KPC/IL17A$^{-/-}$ mice.

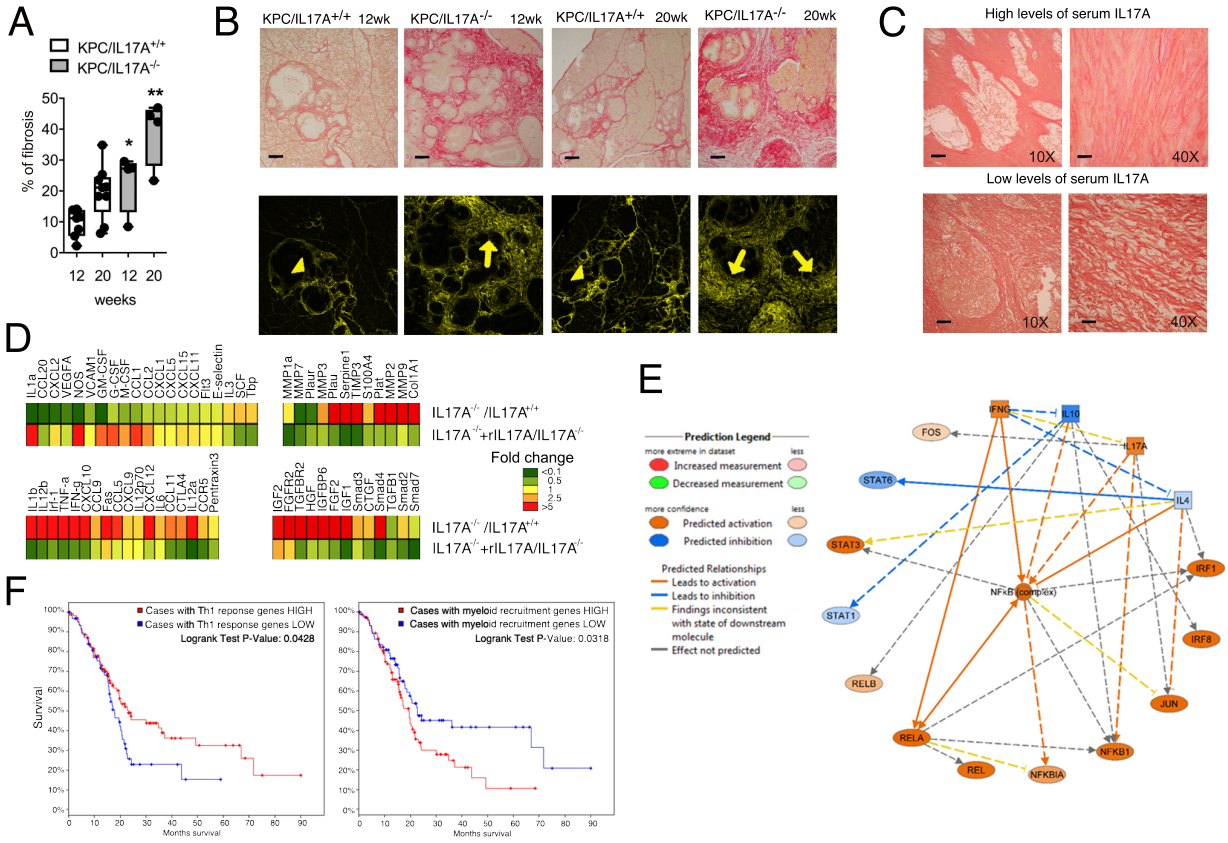
A
KPC/IL17A+/+
KPC/IL17A-/-
% of fibrosis
weeks
B
KPC/IL17A+/+ 12wk
KPC/IL17A-/- 12wk
KPC/IL17A+/+ 20wk
KPC/IL17A-/- 20wk
C
High levels of serum IL17A
Low levels of serum IL17A
10X
40X
D
IL17A-/- /IL17A+/+
IL17A-/-+rIL17A/IL17A-/-
Fold change
E
Prediction Legend
Increased measurement
Decreased measurement
Predicted activation
Predicted inhibition
Predicted Relationships
Leads to activation
Leads to inhibition
Findings inconsistent with state of downstream molecule
Effect not predicted
IFNG
IL10
FOS
IL17A
STAT6
IL4
STAT3
IRF1
NFkB (complex)
STAT1
IRF8
RELB
JUN
RELA
NFKB1
REL
NFKBIA
F
Cases with Th1 reponse genes HIGH
Cases with Th1 response genes LOW
Logrank Test P-Value: 0.0428
Cases with myeloid recruitment genes HIGH
Cases with myeloid recruitment genes LOW
Logrank Test P-Value: 0.0318
Survival
Months survival

Figure 2. Fibroblast clustering and differential immune infiltrate in the presence and absence of IL17A. (*A*) Unsupervised hierarchical clustering analysis of single-cell qPCR data. The color code map represents gene expression after the logarithmic normalization performed by Seurat. (*B*) Dimensional reduction using t-SNE: Cells are colored by genotype (upper plot) and by the four clusters found by Seurat (lower plot). (*C*) Venn diagram of genes differentially expressed between genotypes, between cluster 0 and cluster 3, and between cluster 1 and cluster 2. Alpha-SMA (*D*), F4/80 (*E*), CD3 (*F*), CD8 (*G*) and FoxP3 (*H*) quantification (upper panels) in pancreatic tumor tissues from KPC/IL17A$^{+/+}$ mice (white floating bars) and KPC/IL17A$^{-/-}$ mice (grey floating bars). Each symbol corresponds to a single mouse, and min to max values are represented. **P* < 0.05 and *** *P* < 0.0001 represent significant differences in the IL17A-deficient mice compared to the IL17A-proficient mice; §§ *P* < 0.001 and §§§ *P* < 0.0001 represent differences in the same genotype group of mice compared to 12-week old mice. Middle and lower panels: IHC representative pictures of the above five markers, respectively, with tissues from KPC/IL17A$^{+/+}$ and KPC/IL17A$^{-/-}$ mice at 12 weeks of age. Scale bar represents 100 μm.

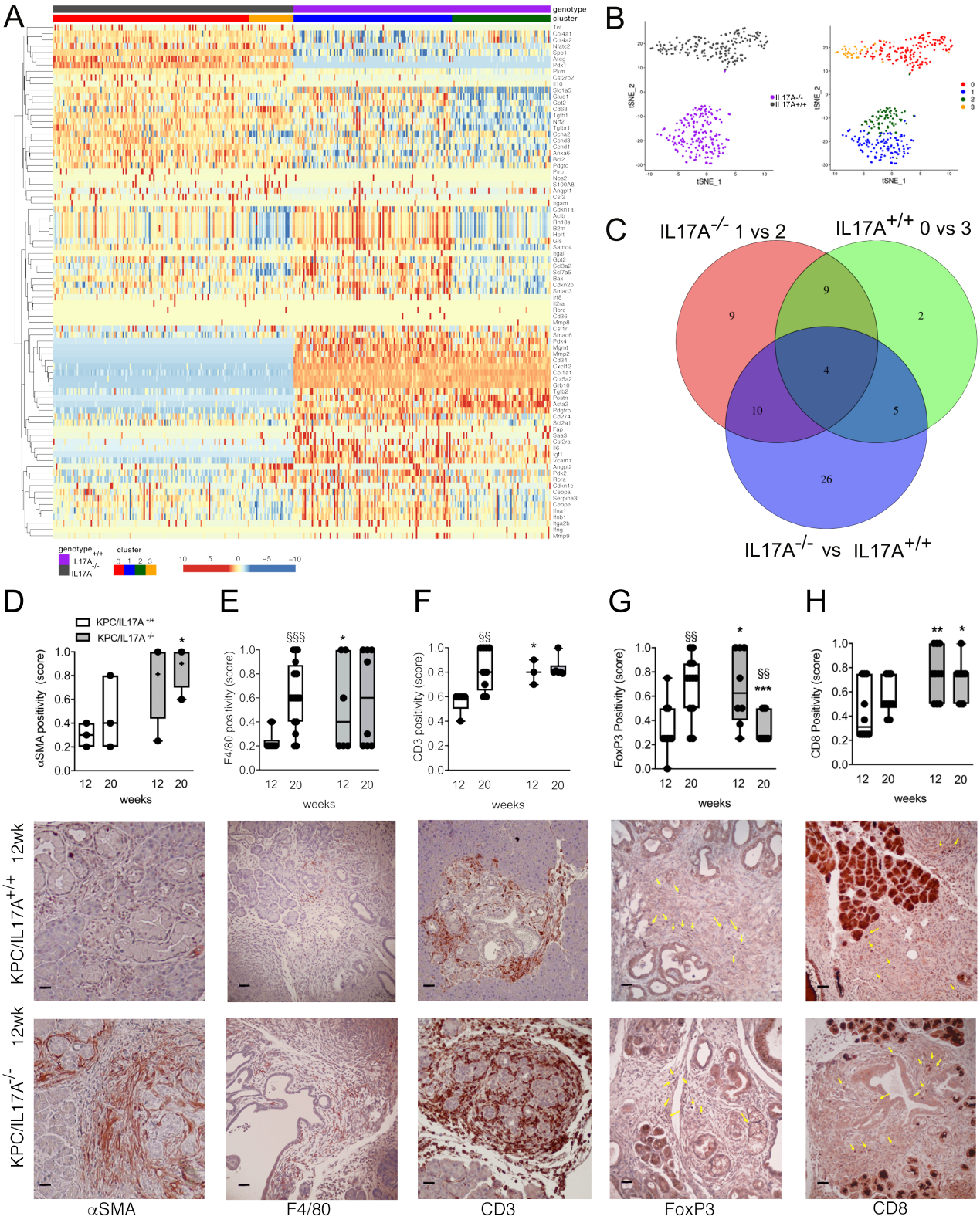
A
genotype
cluster
B
IL17A-/-
IL17A+/+
tSNE_1
tSNE_2
C
IL17A-/- 1 vs 2
IL17A+/+ 0 vs 3
9
9
2
4
10
5
26
IL17A-/- vs IL17A+/+
D
E
F
G
H
KPC/IL17A +/+
KPC/IL17A -/-
αSMA positivity (score)
F4/80 positivity (score)
CD3 positivity (score)
FoxP3 Positivity (score)
CD8 Positivity (score)
weeks
12 20 12 20
KPC/IL17A+/+ 12wk
KPC/IL17A-/- 12wk
αSMA
F4/80
CD3
FoxP3
CD8

Figure 3. IL17A-shaped fibroblasts impair the anti-tumor response. mRNA was isolated from tumor paraffin-embedded tissues from both KPC/IL17A$^{+/+}$ and KPC/IL17A$^{-/-}$ mice (N = 3) (*A*) and from WT mice orthotopically injected with syngeneic PDA cells and untreated or treated with anti-IL17A antibody (N = 5) (*B*) and analyzed by custom arrays for qPCR. *Gapdh* was used as a reference gene. The graph represents the mean fold-change of the indicated genes in KPC/IL17A$^{-/-}$ mice compared to KPC/IL17A$^{+/+}$ mice or in anti-IL17A treated mice compared to untreated mice. Fold-change values are reported in each bar.

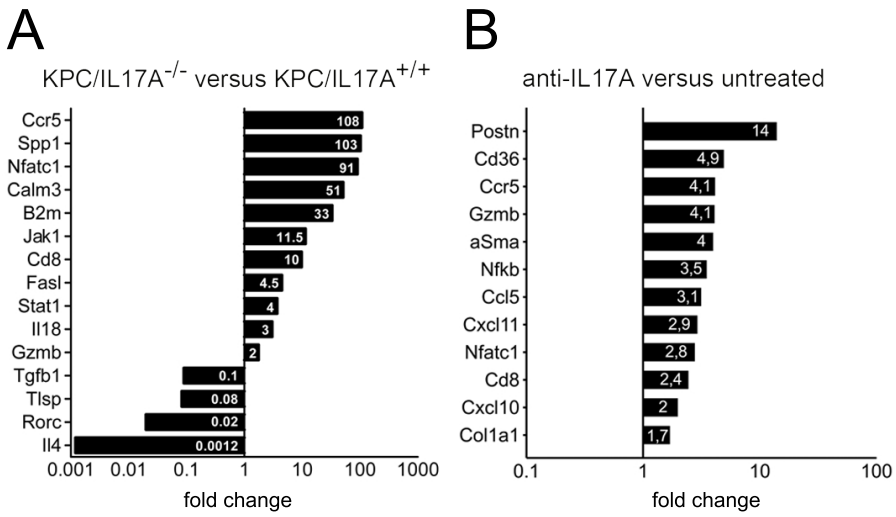

Figure 4. Schematic representation of the IL17A effects on CAFs inside PDA. Tumor microenvironment composition and organization in the presence (left panel) and absence (right panel) of IL17A. The different phenotype acquired by CAFs is highlighted by their different colors (red and yellow when in the presence and absence of IL17A, respectively). Straight or curved grey lines represent the different orientation and accumulation of collagen fibers in the presence and absence of IL17A. Main cytokines/chemokines and factors released by CAFs in the two different scenarios are represented by colored dots, as reported at the bottom of each panel. Differentially attracted immune cells are represented and described in the legend on the right.